Available online at www.sciencedirect.com
ScienceDirect
International Journal of Thermal Sciences 47 (2008) 43–51
International Journal of Thermal Sciences
www.elsevier.com/locate/ijts

# Conjugate forced convection heat transfer in a plane channel: Longitudinally periodic regime

A. Barletta [a,*], E. Rossi di Schio [a], G. Comini [b], P. D'Agaro [b]

[a] *Università di Bologna, Dipartimento di Ingegneria Energetica, Nucleare e del Controllo Ambientale (DIENCA), Laboratorio di Montecuccolino, Via dei Colli 16, 40136 Bologna, Italy*

[b] *Università degli Studi di Udine, Dipartimento di Energetica e Macchine, Via delle Scienze 208, 33100 Udine, Italy*

Received 4 August 2006; received in revised form 12 December 2006; accepted 9 January 2007

Available online 21 February 2007

**Abstract**

The present paper studies the conjugate heat transfer problem in a parallel-plane channel. Laminar and stationary forced convection is studied, with a boundary condition given by a temperature distribution on the external side of the channel wall, which undergoes a sinusoidal longitudinal change. The local energy balance equation is written with reference to the fully developed region, where the temperature distribution can be expressed as a periodic function of the longitudinal coordinate. The temperature field in the solid wall and in the fluid, as well as the local and average Nusselt number, are determined analytically and numerically. A comparison between the values obtained analytically, by employing a complex temperature method, and those evaluated numerically, by employing a Bubnov–Galerkin finite element method, reveals an excellent agreement.



*Keywords:* Forced convection; Laminar flow; Complex temperature; Spatially periodic; Analytical solution; Numerical methods

## 1. Introduction

Periodic boundary conditions, i.e. boundary conditions such that the temperature or the heat flux distribution varies longitudinally with sinusoidal law, deserve great interest in engineering applications. The attention devoted to this subject is due to their applications, such as the design of cooling systems for nuclear reactors, of heat exchangers for Stirling-cycle machines, as well as the analysis of forced convection in internally finned ducts. In the literature on forced convection in ducts, such boundary conditions have already been employed in [1–6], with reference to a heat flux which varies periodically in the longitudinal direction. For instance, Pearlstein and Dempsey [3] report the temperature field, as well as the bulk temperature, in the thermal entrance region of a circular duct, for different values assumed by the Peclet number. The wall heat flux varies longitudinally with sinusoidal or exponential law. In [5,6], forced convection flow is studied, both by neglecting and by taking into account the fluid axial conduction effect, with reference to the fully developed region of a cylindrical duct with circular cross-section. The boundary condition considered is given by a wall heat flux distribution which varies axially with a sinusoidal law. It is shown that, in the fully developed region, the temperature distribution can be expressed as the sum of a linear and a periodic function of the axial coordinate. In none of the above mentioned papers, the coupling with the heat conduction in the wall is taken into account.

The aim of the present paper is to study the conjugate problem of forced convection in a parallel-plane channel, i.e. by considering also the effect of heat conduction in the channel walls. The boundary condition, that is prescribed on the external boundary of the channel wall, is given by a temperature distribution expressed by a periodic function of the longitudinal coordinate, with average value $T_0$. The longitudinal heat conduction and the viscous dissipation in the fluid will be neglected. Reference will be made to the hydrodynamically and thermally developed region. The local energy balance equation will be solved analytically and numerically both for the fluid

* Corresponding author. Tel.: +39 051 6441703; fax: +39 051 6441747.
*E-mail address:* antonio.barletta@mail.ing.unibo.it (A. Barletta).

1290-0729/$ – see front matter 
doi:10.1016/j.ijthermalsci.2007.01.013

**Nomenclature**

| | |
|---|---|
| $\mathbf{A}$ | dimensionless convection matrix, defined in Eq. (39) |
| $B$ | dimensionless angular frequency, defined in Eq. (6) |
| $C_1$, $C_2$, $C_3$ | constants, defined in Eq. (18) |
| ${}_1F_1$ | confluent hypergeometric function |
| $G$ | complex dimensionless parameter |
| $H$ | complex dimensionless parameter |
| $i$ | complex unit |
| $k$ | thermal conductivity |
| $\mathbf{K}$ | dimensionless conduction matrix, defined in Eq. (39) |
| $L$ | length of the computational domain |
| $M, m, n$ | positive integers |
| $\mathbf{N}$ | vector of the interpolating functions, defined in Eq. (38) |
| $Nu$ | Nusselt number, defined by Eq. (20) |
| $\overline{Nu}$ | average value of the Nusselt number in a longitudinal period, defined by Eq. (29) |
| $p$ | order of the approximating function |
| $Pe$ | Peclet number, defined in Eq. (6) |
| $r$ | refinement factor |
| $t$ | time |
| $T$ | temperature |
| $\mathbf{u}$ | dimensionless velocity |
| $U$ | longitudinal component of the fluid velocity |
| $U_0$ | mean value of the fluid velocity |
| $u$ | dimensionless longitudinal component of the fluid velocity |
| $\mathbf{x}$ | vector defined in Eq. (39) |
| $y$ | spatial coordinate |
| $y_0$ | half-distance between the channel walls |
| $y_1$ | half-width of the full channel |
| $W$ | complex dimensionless function |
| $z$ | longitudinal coordinate |

*Greek symbols*

| | |
|---|---|
| $\alpha$ | thermal diffusivity |
| $\beta$ | angular frequency |
| $\gamma$ | dimensionless parameter, defined in Eq. (6) |
| $\Delta E$ | numerical accuracy, defined in Eq. (42) |
| $\Delta T$ | oscillation amplitude of the boundary temperature |
| $\zeta$ | dimensionless longitudinal coordinate, defined in Eq. (6) |
| $\zeta_n$ | dimensionless constants defined in Eq. (28), |
| $\eta$ | dimensionless spatial coordinate, defined in Eq. (6) |
| $\theta$ | dimensionless temperature, defined in Eq. (6) |
| $\hat{\theta}$ | dimensionless temperature, defined in Eq. (36) |
| $\theta_0$, $\theta_1$, $\theta_2$ | dimensionless functions, defined in Eq. (11) |
| $\mathbf{\Theta}$ | dimensionless temperature vector, defined in Eq. (38) |
| $\sigma$ | dimensionless half-width of the full channel, defined in Eq. (6) |
| $\varphi$ | dimensionless heat flux, defined in Eq. (22) |
| $\varphi_1$, $\varphi_2$ | dimensionless parameters, defined in Eq. (22) |
| $\phi$ | dimensionless complex heat flux, defined in Eq. (26) |
| $\psi$ | complex dimensionless temperature |
| $\Omega$ | computational domain |

*Operators*

| | |
|---|---|
| $\nabla$ | dimensionless gradient |

*Subscripts*

| | |
|---|---|
| $b$ | bulk quantity |
| $C$ | coarse mesh |
| $f$ | fluid |
| $F$ | fine mesh |
| $s$ | solid |

and for the solid region. The fluid temperature distribution will be obtained analytically by expressing the energy balance equation as a complex-valued hypergeometric confluent equation. The numerical solution for the temperature field, both in the fluid and in the solid region, will be obtained according to the finite element computational procedure described in [7–11].

## 2. Mathematical model

In the present section, the local energy balance equation, written separately for the solid region and for the fluid region, is solved analytically with the boundary condition given by a temperature distribution which varies longitudinally with sinusoidal law.

Let us consider an infinite plane-parallel channel, such that the walls, with distance $2y_0$, have thickness $y_1 - y_0$. Since a symmetry with reference to the $y = 0$ plane occurs, it is possible to study only half of the domain: $0 \leqslant y \leqslant y_1$. A drawing

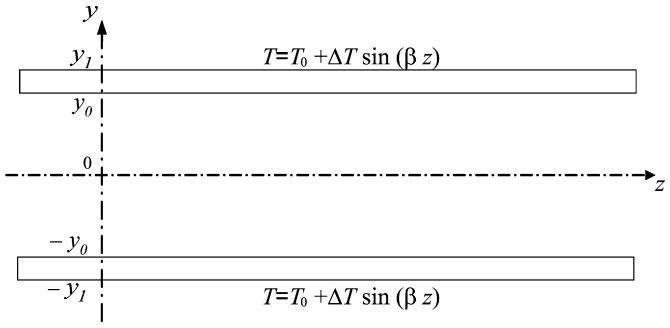


Fig. 1. Drawing of the longitudinal section of the channel.

of the section of the parallel-plane channel, together with the boundary condition, is reported in Fig. 1.

Let us consider the fully developed forced convection of a Newtonian fluid, with constant thermophysical properties, and such that viscous dissipation and longitudinal heat conduction effects can be neglected. Moreover, let us assume that the ex-

ternal boundaries of the channel, $y = \pm y_1$, are subjected to a temperature distribution $T(\pm y_1, z) = T_0 + \Delta T \sin(\beta z)$.

In the fully developed region, the local energy balance equation for the fluid region ($0 \leqslant y \leqslant y_0$) is given by

$$U\frac{\partial T}{\partial z} = \alpha_f \frac{\partial^2 T}{\partial y^2} \tag{1}$$

while for the solid region ($y_0 \leqslant y \leqslant y_1$) it can be expressed as

$$\frac{\partial^2 T}{\partial y^2} + \frac{\partial^2 T}{\partial z^2} = 0 \tag{2}$$

where the subscript $f$ is for fluid and $U(y)$ is the Poiseuille velocity distribution:

$$U(y) = \frac{3U_0}{2}\left[1 - \left(\frac{y}{y_0}\right)^2\right] \tag{3}$$

The equations must be solved together with the boundary condition, as well as with the symmetry condition in $y = 0$

$$\left.\frac{\partial T}{\partial y}\right|_{y=0} = 0 \tag{4}$$

and with the matching conditions in $y = y_0$, namely

$$T_f(y_0, z) = T_s(y_0, z), \qquad k_f \left.\frac{\partial T}{\partial y}\right|_{f, y=y_0} = k_s \left.\frac{\partial T}{\partial y}\right|_{s, y=y_0} \tag{5}$$

where the subscript $f$ refers to the fluid while the subscript $s$ refers to the solid. Let us introduce the following dimensionless quantities:

$$\eta = \frac{y}{y_0}, \quad \zeta = \frac{z}{y_0}, \quad \sigma = \frac{y_1}{y_0}, \quad \theta = \frac{T - T_0}{\Delta T}$$
$$\gamma = \frac{k_s}{k_f}, \quad Pe = \frac{U_0 y_0}{\alpha_f}, \quad B = Pe\beta y_0, \quad u = \frac{U}{U_0} \tag{6}$$

It is thus possible to write the dimensionless local balance equations, for the fluid region and for the solid region, respectively as

$$u\frac{\partial \theta}{\partial \zeta} = \frac{1}{Pe}\frac{\partial^2 \theta}{\partial \eta^2}, \quad 0 < \eta < 1$$
$$\frac{\partial^2 \theta}{\partial \eta^2} + \frac{\partial^2 \theta}{\partial \zeta^2} = 0, \quad 1 < \eta < \sigma \tag{7}$$

with the boundary condition

$$\theta(\sigma, \zeta) = \sin\left(\frac{B\zeta}{Pe}\right) \tag{8}$$

with the symmetry condition in $\eta = 0$

$$\left.\frac{\partial \theta}{\partial \eta}\right|_{\eta=0} = 0 \tag{9}$$

and with the matching conditions in $\eta = 1$

$$\theta_f(1, \zeta) = \theta_s(1, \zeta), \quad \left.\frac{\partial \theta}{\partial \eta}\right|_{f, \eta=1} = \gamma \left.\frac{\partial \theta}{\partial \eta}\right|_{s, \eta=1} \tag{10}$$

## 3. Analytical solution

At longitudinal positions sufficiently far from the inlet section of the duct, the solution of Eq. (7) can be written as

$$\theta(\eta, \zeta) = \theta_0(\eta) + \theta_1(\eta)\sin\left(\frac{B\zeta}{Pe}\right) + \theta_2(\eta)\cos\left(\frac{B\zeta}{Pe}\right) \tag{11}$$

where the functions $\theta_0(\eta)$, $\theta_1(\eta)$ and $\theta_2(\eta)$ can be determined by substituting Eq. (11) into Eqs.(7)–(10). In fact, one obtains three boundary value problems:

$$\begin{cases} 0 < \eta < 1 \quad \Rightarrow \quad \mathrm{d}^2\theta_0(\eta)/\mathrm{d}\eta^2 = 0 \\ 1 < \eta < \sigma \quad \Rightarrow \quad \mathrm{d}^2\theta_0(\eta)/\mathrm{d}\eta^2 = 0 \\ \mathrm{d}\theta_0/\mathrm{d}\eta|_{\eta=0} = 0 \\ \theta_{0,f}(1) = \theta_{0,s}(1) \\ \mathrm{d}\theta_0/\mathrm{d}\eta|_{f,\eta=1} = \gamma\, \mathrm{d}\theta_0/\mathrm{d}\eta|_{s,\eta=1} \\ \theta_0(\sigma) = 0 \end{cases} \tag{12}$$

$$\begin{cases} 0 < \eta < 1 \quad \Rightarrow \quad \mathrm{d}^2\theta_1(\eta)/\mathrm{d}\eta^2 = -u(\eta)B\theta_2(\eta) \\ 1 < \eta < \sigma \quad \Rightarrow \quad \mathrm{d}^2\theta_1(\eta)/\mathrm{d}\eta^2 = (B^2/Pe^2)\theta_1(\eta) \\ \mathrm{d}\theta_1/\mathrm{d}\eta|_{\eta=0} = 0 \\ \theta_{1,f}(1) = \theta_{1,s}(1) \\ \theta_1/\mathrm{d}\eta|_{f,\eta=1} = \gamma\, \mathrm{d}\theta_1/\mathrm{d}\eta|_{s,\eta=1} \\ \theta_1(\sigma) = 1 \end{cases} \tag{13}$$

$$\begin{cases} 0 < \eta < 1 \quad \Rightarrow \quad \mathrm{d}^2\theta_2(\eta)/\mathrm{d}\eta^2 = u(\eta)B\theta_1(\eta) \\ 1 < \eta < \sigma \quad \Rightarrow \quad \mathrm{d}^2\theta_2(\eta)/\mathrm{d}\eta^2 = (B^2/Pe^2)\theta_2(\eta) \\ \mathrm{d}\theta_2/\mathrm{d}\eta|_{\eta=0} = 0 \\ \theta_{2,f}(1) = \theta_{2,s}(1) \\ \mathrm{d}\theta_2/\mathrm{d}\eta|_{f,\eta=1} = \gamma\, \mathrm{d}\theta_2/\mathrm{d}\eta|_{s,\eta=1} \\ \theta_2(\sigma) = 0 \end{cases} \tag{14}$$

If one introduces the complex valued function $\psi(\eta) = \theta_1(\eta) + i\theta_2(\eta)$, Eqs. (13) and (14) can be collapsed into a unique boundary value problem. By employing Eq. (3), one obtains:

$$\begin{cases} 0 < \eta < 1 \quad \Rightarrow \quad \mathrm{d}^2\psi(\eta)/\mathrm{d}\eta^2 - (3/2)iB(1-\eta^2)\psi(\eta) = 0 \\ 1 < \eta < \sigma \quad \Rightarrow \quad \mathrm{d}^2\psi(\eta)/\mathrm{d}\eta^2 - (B^2/Pe^2)\psi(\eta) = 0 \\ \mathrm{d}\psi/\mathrm{d}\eta|_{\eta=0} = 0 \\ \psi_f(1) = \psi_s(1) \\ \mathrm{d}\psi/\mathrm{d}\eta|_{f,\eta=1} = \gamma\, \mathrm{d}\psi/\mathrm{d}\eta|_{s,\eta=1} \\ \psi(\sigma) = 1 \end{cases} \tag{15}$$

The solution of the boundary value problem (12) yields $\theta_0(\eta) = 0$. The solution of the boundary value problem (15) allows one to determine the temperature field for the fluid and the solid region separately.

For the fluid region, $0 < \eta < 1$, on account of the symmetry condition in $\eta = 0$, one obtains

$$\psi(\eta) = C_1 e^{H\eta^2/4}\, {}_1F_1\left(\frac{2+H}{8}; \frac{1}{2}; -\frac{H}{2}\eta^2\right) \tag{16}$$

where $H = (i-1)\sqrt{3B}$ and $C_1$ is an integration constant to be determined by employing the matching conditions. The complex temperature $\psi$ depends on the parameters $\sigma$, $\gamma$ and $Pe$ through the constant $C_1$.

For the solid region, $1 < \eta < \sigma$, one has

$$\psi(\eta) = C_2 e^{\eta B/Pe} + C_3 e^{-\eta B/Pe} \tag{17}$$

where the integration constants can be determined by prescribing the boundary condition in $\eta = \sigma$ and the matching conditions, thus obtaining

$$\begin{aligned} C_1 &= \left\{e^{B(1-\sigma)/Pe} + C_3\left[e^{-B/Pe} - e^{B(1-2\sigma)/Pe}\right]\right\} \\ &\quad \times \left[{}_1F_1\left(\frac{2+H}{8}; \frac{1}{2}; -\frac{H}{2}\right)e^{H/4}\right]^{-1} \\ C_2 &= e^{-\sigma B/Pe} - C_3 e^{-2\sigma B/Pe} \\ C_3 &= \left[\frac{B\gamma}{Pe}e^{-B/Pe}e^{-B(\sigma-2)/Pe} + e^{B(1-\sigma)/Pe}\left(G - \frac{H}{2}\right)\right] \\ &\quad \times \left[e^{-B/Pe}\left[\left(\frac{H}{2} - G\right)\left(1 - e^{2B(1-\sigma)/Pe}\right)\right.\right. \\ &\quad \left.\left. + \frac{B\gamma}{Pe}\left(1 + e^{2B(1-\sigma)/Pe}\right)\right]\right]^{-1} \end{aligned} \tag{18}$$

where the parameter

$$\begin{aligned} G &= \frac{1}{4}H(2+H){}_1F_1\left(\frac{10+H}{8}; \frac{3}{2}; -\frac{H}{2}\right) \\ &\quad \times \left[{}_1F_1\left(\frac{2+H}{8}; \frac{1}{2}; -\frac{H}{2}\right)\right]^{-1} \end{aligned} \tag{19}$$

has been employed.

By employing the dimensionless quantities, one can express the Nusselt number as

$$\begin{aligned} Nu &= y_0 \left.\frac{\partial T}{\partial y}\right|_{f, y=y_0} \left[T(y_0, z) - T_b(z)\right]^{-1} \\ &= -\frac{\varphi(\zeta)}{\theta(1,\zeta) - \theta_b(\zeta)} \end{aligned} \tag{20}$$

where $\theta_b$ is the dimensionless bulk temperature,

$$\theta_b(\zeta) = \frac{3}{2}\int_0^1 \theta(\eta, \zeta)\left(1 - \eta^2\right) \mathrm{d}\eta \tag{21}$$

and $\varphi(\zeta)$ is the dimensionless heat flux at the solid–fluid interface, namely

$$\begin{aligned} \varphi(\zeta) &= -\left.\frac{\partial\theta}{\partial\eta}\right|_{f,\eta=1} \\ &= -\left.\frac{\mathrm{d}\theta_1}{\mathrm{d}\eta}\right|_{f,\eta=1} \sin\left(\frac{B\zeta}{Pe}\right) - \left.\frac{\mathrm{d}\theta_2}{\mathrm{d}\eta}\right|_{f,\eta=1} \cos\left(\frac{B\zeta}{Pe}\right) \\ &= \varphi_1 \sin\left(\frac{B\zeta}{Pe}\right) + \varphi_2 \cos\left(\frac{B\zeta}{Pe}\right) \end{aligned} \tag{22}$$

On account of Eqs. (11) and (22), the local Nusselt number can be rewritten as

$$\begin{aligned} &Nu(\zeta) \\ &= -\frac{\varphi_1 \sin(B\zeta/Pe) + \varphi_2 \cos(B\zeta/Pe)}{[\theta_1(1) - \theta_{1b}]\sin(B\zeta/Pe) + [\theta_2(1) - \theta_{2b}]\cos(B\zeta/Pe)} \end{aligned} \tag{23}$$

where $\theta_{1b}$ and $\theta_{2b}$ are respectively the real and the imaginary part of

$$\psi_b = \frac{3}{2}\int_0^1 \psi(\eta)\left(1 - \eta^2\right) \mathrm{d}\eta \tag{24}$$

An integration of the first equation which appears in Eq. (15) yields

$$\psi_b = -\frac{i}{B}\left.\frac{\mathrm{d}\psi}{\mathrm{d}\eta}\right|_{f,\eta=1} = \frac{i}{B}\phi \tag{25}$$

where $\phi = \varphi_1 + i\varphi_2$ is the complex dimensionless heat flux at the interface, defined as

$$\phi = -\left.\frac{\mathrm{d}\psi}{\mathrm{d}\eta}\right|_{f,\eta=1} \tag{26}$$

On account of Eq. (25) one can express the Nusselt number as

$$\begin{aligned} &Nu(\zeta) \\ &= \frac{-B[\varphi_1 \sin(B\zeta/Pe) + \varphi_2 \cos(B\zeta/Pe)]}{[B\theta_1(1) + \varphi_2]\sin(B\zeta/Pe) + [B\theta_2(1) - \varphi_1]\cos(B\zeta/Pe)} \end{aligned} \tag{27}$$

The Nusselt number expressed by Eq. (27) displays singularities for all those longitudinal positions $\zeta_n$ such that $\theta(1, \zeta) = \theta_b(\zeta)$, i.e. for all the positions

$$\zeta_n = -\frac{Pe}{B}\arctan\left(\frac{B\theta_2(1) - \varphi_1}{B\theta_1(1) + \varphi_2}\right) + \frac{\pi n Pe}{B} \tag{28}$$

for every positive integer $n$. The average value of the Nusselt number in a longitudinal period is given by

$$\overline{Nu} = \frac{B}{2\pi Pe}\int_0^{2\pi\, Pe/B} Nu(\zeta)\, \mathrm{d}\zeta \tag{29}$$

On account of the singularities which affect the local Nusselt number, the integral which appears in Eq. (29) is ill defined. However its principal value exists and is given by

$$\overline{Nu} = -\frac{\varphi_1[B\theta_1(1) + \varphi_2] + \varphi_2[B\theta_2(1) - \varphi_1]}{[B\theta_1(1) + \varphi_2]^2 + [B\theta_2(1) - \varphi_1]^2} \tag{30}$$

It is possible to rewrite Eq. (30) as

$$\overline{Nu} = \frac{B^2}{2|B\psi(1) - i\phi|^2}\left.\frac{\mathrm{d}}{\mathrm{d}\eta}|\psi|^2\right|_{f,\eta=1} \tag{31}$$

Eq. (31) shows that the average Nusselt number depends only on the parameter $B$.

A remarkable special case is represented by the limit $Pe \to \infty$. In this case, the analytical solution becomes simpler. In fact, if one fixes the value of $B$ and lets the parameter $Pe$ tend to infinity, one obtains the following expression for the complex temperature:

$$\begin{aligned} &0 < \eta < 1 \quad \Rightarrow \\ &\psi(\eta) = \frac{2\gamma e^{-H(1-\eta^2)/4}}{W(\sigma)}{}_1F_1\left(\frac{2+H}{8}; \frac{1}{2}; -\frac{H}{2}\eta^2\right) \\ &\quad \times \left[{}_1F_1\left(\frac{2+H}{8}; \frac{1}{2}; -\frac{H}{2}\right)\right]^{-1} \end{aligned} \tag{32}$$

$$1 < \eta < \sigma \quad \Rightarrow \quad \psi(\eta) = \frac{W(\eta)}{W(\sigma)} \tag{33}$$

where the function

$$W(\eta) = 2\gamma + (\eta - 1)[H - 2G] \tag{34}$$

is employed.

## 4. Numerical solution

The energy balance equation for a fluid with constant thermophysical properties, with no heat sources, in stationary regime and by neglecting the effect of viscous dissipation, can be written in a dimensionless form as follows:

$$(\mathbf{u} \cdot \nabla)\theta = \frac{1}{Pe}\nabla^2\theta \tag{35}$$

In a conjugate heat transfer problem, Eq. (35) is solved for the whole domain by assuming, for each region (solid and fluid) the corresponding thermophysical properties and by prescribing $\mathbf{u} = 0$ in the solid region. Indeed, the continuity of the temperature at the solid–fluid interface is ensured by the energy equation itself, and it is not necessary to prescribe it explicitly [11].

The computational domain is a portion of plane channel in the thermally developed region; the considered portion of channel has length $L = 2\pi/\beta$, which corresponds to an oscillation period of the sinusoidal external wall temperature (Eq. (8)).

As in the analytical solution, the symmetry condition allows one to consider only half computational domain.

In order to prescribe the periodic boundary conditions on the inlet and outlet sections of the computational domain, one can define a dimensionless temperature as [10]

$$\hat{\theta}(\eta, \zeta) = \frac{\theta(\eta, \zeta) - \theta(1, \zeta)}{\theta_b(\zeta) - \theta(1, \zeta)} \tag{36}$$

The periodicity of the function $\hat{\theta}(\eta, \zeta)$ implies that

$$\hat{\theta}(\eta, 0) = \hat{\theta}\left(\eta, \frac{2\pi Pe}{B}\right) \tag{37}$$

In the approximation of Eq. (35), we express the temperature distribution by means of the usual expansion

$$\theta \cong \sum_{m=1}^{M} N_m \theta_m = \mathbf{N}\boldsymbol{\Theta} \tag{38}$$

where $\theta_m$ are the nodal values of temperature and $N_m$ are the interpolating functions. Eq. (38) is substituted into Eq. (35) and, in accordance with the Bubnov–Galerkin method, the weighting functions for each node are chosen to be same as the interpolating functions $N_m$. In this way the numerical diffusivity, which typically arises in the up-wind schemes, is avoided [9]. Since the analytical expression of the velocity is known from Eq. (3), the standard steps of the Bubnov–Galerkin method yield a non-symmetric system of discretized equations in which the only unknowns are either the nodal temperatures or the nodal rates of heat transfer through the walls where the boundary conditions of the first kind are prescribed. This system can be written in matrix form as

$$(\mathbf{K} + \mathbf{A})\boldsymbol{\Theta} = \mathbf{x} \tag{39}$$

where $\mathbf{K}$ is the conduction matrix, $\mathbf{A}$ is the convection matrix, and $\mathbf{x}$ is the vector of unknown rates of heat transfer through the walls where the boundary conditions of the first kind are prescribed [7, Chapter 5]. With reference to the whole computational domain $\Omega$, the matrix entries in the conduction and convection matrices are defined as

$$K_{n,m} = \frac{1}{Pe}\int_{\Omega} \nabla N_n \cdot \nabla N_m \, \mathrm{d}\Omega \tag{40}$$

$$A_{n,m} = \int_{\Omega} N_n \mathbf{u} \cdot \nabla N_m \, \mathrm{d}\Omega \tag{41}$$

for $n, m = 1, M$. The entries $x_m$ in the vector $\mathbf{x}$, are not written explicitly since they are never input as applied loads, but are evaluated as "reactions" after a complete temperature solution is obtained [7, pp. 151–153].

The periodicity conditions at inflow and outflow boundaries imply a coupling between corresponding nodal points, which effectively reduces the number of unknown temperatures. In the finite element solution, the coupling between corresponding nodal points is usually accomplished by manipulating the lists of nodal connections [10]. After a complete temperature solution of the reduced system is obtained, not only the reactions but also the heat transfer rates through the solid–fluid interface can be easily evaluated by means of the procedure illustrated in [8]. Finally, it might be of some interest to note that the non-symmetric systems of algebraic equations arising from the discretization process are solved very efficiently by the conjugate gradient squared (CGS) method illustrated in [9].

### 4.1. Validation

Simulations have been done for $Pe = 100$ and $\sigma = 1.2$, for different values assumed by the dimensionless parameter $B$ (in the range $B = 1 \div 100$) and two different values assumed by the parameter $\gamma$ ($\gamma = 0.5, 3$).

In the nondimensional domain, the computational grid has height 1 and axial length ranging from $20\pi$ (for $B = 1$) to $\pi$ (for $B = 100$). Uniform spacings have been assumed in both the axial and the transverse directions. As it will be apparent in the following, this choice has several practical advantages whenever computer resources allow the use of very large numbers of nodal points. In the axial direction, a constant number of 501 equally spaced nodes has been applied to the range $B = 5 \div 100$. For the cases $B = 1$ and $B = 2$ the number of nodes in the axial direction has been increased to 1501 and 3001 respectively, in order to maintain the length/height aspect ratio of the elements below 7. As far as the accuracy is concerned, the most critical issue is the fineness of the domain subdivision in the transverse direction. Therefore, the refinement of the mesh was done in the transverse direction, progressively increasing the number of grid points from 16 to 31.

The formal order of accuracy $\Delta E$ achieved with the finite element approximation can be estimated, in the present case of negligible errors in the longitudinal direction, using the expression

$$\Delta E = \mathrm{O}\left[(\Delta y)^{p+1}\right] \tag{42}$$

where $\Delta y$ is the transverse distance between nodal points and $p$ is the order of the approximating function [7, pp. 124–125]. For a uniform mesh, the relative accuracy can be express as

$$\Delta E/E = \mathrm{O}\left[(\Delta y/y_1)^{p+1}\right] \tag{43}$$

with reference to the width of the domain $y_1$. Thus we can say that, with the linear approximating functions used here and 30 elements in the transverse direction, the relative accuracy reached for the unknown temperature solution is of the order of

$$\Delta E/E \cong (1/30)^2 = 1.1 \cdot 10^{-3}$$

The observed order of accuracy can be conveniently estimated through the standard Richardson extrapolation [12]. In the present case, with a second order discretization scheme used to produce numerical solutions on two uniformly spaced meshes, the relative order of accuracy can be expressed as

$$\frac{\Delta|\psi(1)|}{|\psi(1)|_F} = \frac{1 - |\psi(1)|_C/|\psi(1)|_F}{r^{p+1} - 1} \tag{44}$$

where the subscripts $F$ and $C$ denote the fine and the coarse mesh respectively, $|\psi(1)|$ denotes the oscillation amplitude of the interface temperature, and $r = \Delta y_C/\Delta y_F$ represents the refinement factor. For $p = 1$, a 31-point fine mesh, a 16-point coarse mesh, and numerically estimated values of the order $1 - |\psi(1)|_C/|\psi(1)|_F \cong 2 \cdot 10^{-3}$, it has been obtained

$$\frac{\Delta|\psi(1)|}{|\psi(1)|_F} = \frac{2.9 \cdot 10^{-3}}{2^2 - 1} \cong 0.7 \cdot 10^{-3}$$

i.e. a relative accuracy of the order of 0.1% for the oscillation amplitude of the interface temperatures.

## 5. Discussion of the results

In Figs. 2 and 3, three-dimensional plots of the dimensionless temperature distribution are reported, versus $\eta$ and $\zeta$, for $B = 100$, $Pe = 100$, $\sigma = 1.2$. Fig. 2 refers to $\gamma = 0.5$, while Fig. 3 refers to $\gamma = 3$. A comparison between the two figures shows how the conductivity of the channel wall affects the temperature distribution. In fact, the temperature gradient in the duct wall is higher in the case of a less conductive solid (Fig. 2). This behavior is expected, since in the limit of an infinitely conducting wall one can neglect the transverse temperature change in the duct and prescribe the boundary condition directly on the solid–fluid interface. Indeed, in this limit the conjugate heat transfer problem reduces to a pure convection problem.

In Fig. 4, the dimensionless temperature distribution at the solid–fluid interface is reported for $Pe = 100$, $\sigma = 1.2$, $\gamma = 3$ and for three different values assumed by the parameter $B$. The figure shows that the period of the axial temperature distribution strongly differs in the three considered cases, while the oscillation amplitude does not display strong differences.

The oscillation amplitude of the interface temperature is reported in Tables 1 and 2, for $\sigma = 1.2$ and for different values assumed by the parameters $B$ and $Pe$. Table 1 refers to $\gamma = 0.5$,

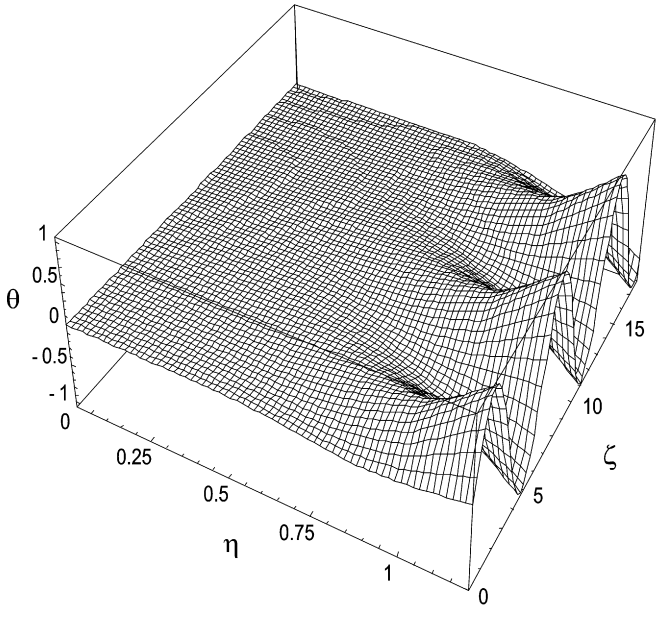


Fig. 2. Analytical solution: dimensionless temperature distribution versus $\eta$ and $\zeta$ for $\sigma = 1.2$, $B = 100$, $Pe = 100$ and $\gamma = 0.5$.

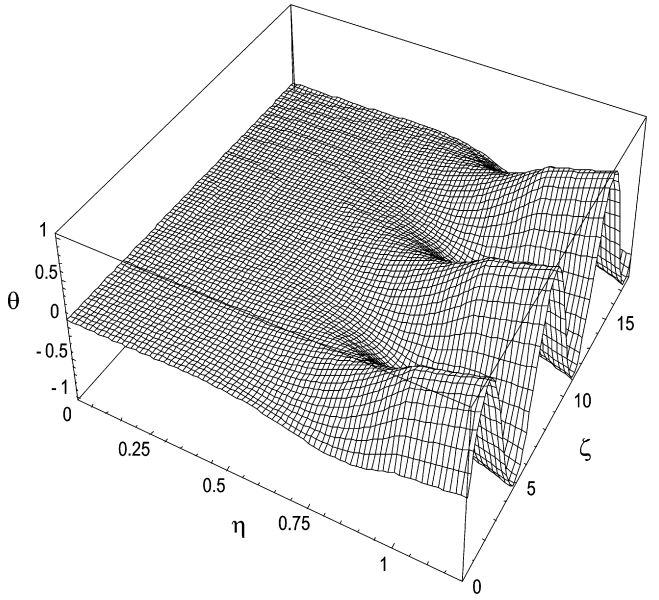


Fig. 3. Analytical solution: dimensionless temperature distribution versus $\eta$ and $\zeta$ for $\sigma = 1.2$, $B = 100$, $Pe = 100$ and $\gamma = 3$.

Table 1
Analytical solution: oscillation amplitude of the temperature in $\eta = 1$, for $\sigma = 1.2$ and $\gamma = 0.5$

| $B$ | $\lvert\psi(1)\rvert$ $Pe = 20$ | $\lvert\psi(1)\rvert$ $Pe = 50$ | $\lvert\psi(1)\rvert$ $Pe = 100$ | $\lvert\psi(1)\rvert$ $Pe \to \infty$ |
|---|---|---|---|---|
| 1 | 0.836442 | 0.836473 | 0.836477 | 0.836479 |
| 2 | 0.699564 | 0.699656 | 0.699669 | 0.699673 |
| 5 | 0.596001 | 0.596452 | 0.596516 | 0.596538 |
| 10 | 0.549786 | 0.551380 | 0.551608 | 0.551684 |
| 20 | 0.487714 | 0.493043 | 0.493811 | 0.494068 |
| 50 | 0.383053 | 0.407164 | 0.410792 | 0.412012 |
| 100 | 0.272835 | 0.338980 | 0.350305 | 0.354204 |
| 200 | 0.127024 | 0.256220 | 0.288646 | 0.300781 |
| 500 | 0.00839573 | 0.106051 | 0.189718 | 0.238308 |
| 1000 | 0.0000659737 | 0.0185782 | 0.0910994 | 0.197655 |

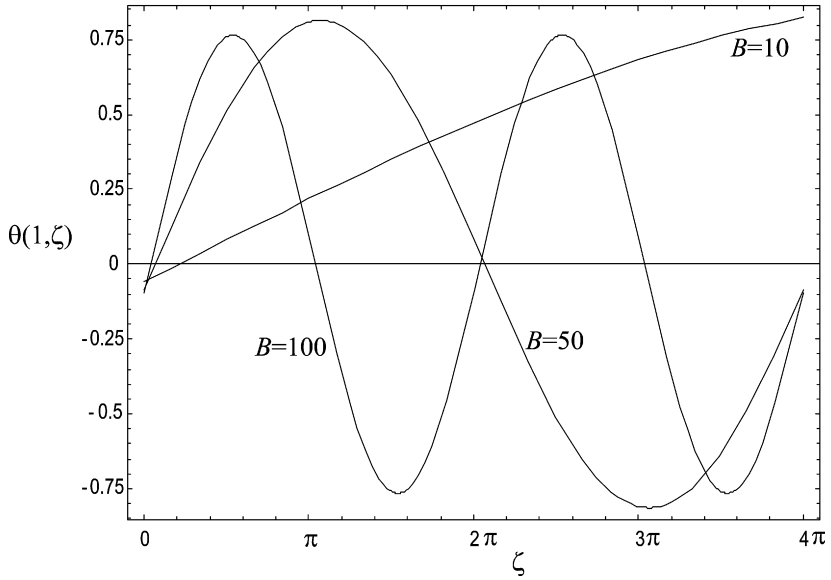


Fig. 4. Analytical solution: dimensionless temperature distribution in $\eta = 1$ for $\sigma = 1.2$, $\gamma = 3$, $Pe = 100$ and for three different values assumed by the parameter $B$.

Table 2
Analytical solution: oscillation amplitude of the temperature in $\eta = 1$, for $\sigma = 1.2$ and $\gamma = 3$

| $B$ | $\lvert\psi(1)\rvert$ $Pe = 20$ | $\lvert\psi(1)\rvert$ $Pe = 50$ | $\lvert\psi(1)\rvert$ $Pe = 100$ | $\lvert\psi(1)\rvert$ $Pe \to \infty$ |
|---|---|---|---|---|
| 1 | 0.973949 | 0.973989 | 0.973995 | 0.973997 |
| 2 | 0.940050 | 0.940202 | 0.940223 | 0.940230 |
| 5 | 0.902568 | 0.903454 | 0.903580 | 0.903622 |
| 10 | 0.881926 | 0.885345 | 0.885835 | 0.885998 |
| 20 | 0.846025 | 0.858909 | 0.860776 | 0.861400 |
| 50 | 0.735259 | 0.803248 | 0.813790 | 0.817354 |
| 100 | 0.533107 | 0.728086 | 0.765105 | 0.778122 |
| 200 | 0.226802 | 0.575100 | 0.687828 | 0.733353 |
| 500 | 0.0122905 | 0.215009 | 0.470245 | 0.666231 |
| 1000 | 0.0000856116 | 0.0317519 | 0.204409 | 0.610435 |

while Table 2 refers to $\gamma = 3$. The tables show that, for fixed values of $Pe$, the amplitude is a decreasing monotonic function of $B$, and that the dependence on $B$ is weaker for increasing values of $Pe$. For fixed values of $B$, the oscillation amplitude of the interface temperature is an increasing monotonic function of $Pe$, in particular for high values of $B$. Both Tables 1 and 2 show that, at least for $B < 100$, the discrepancy between the cases $Pe = 100$ and $Pe \to \infty$ is very small. The decrease of the oscillation amplitude of the temperature field at internal points is a characteristic phenomenon of the steady periodic regime in systems governed by diffusion equations. This feature is less evident for higher values assumed by the Peclet number. The reduction of the oscillation amplitude of the temperature field, for increasing values of $B$, can be interpreted as a reduction of the penetration depth of the oscillations in the transverse direction.

In Table 3, values of the mean Nusselt number, evaluated through Eq. (29), are reported versus $B$. The table shows that the mean Nusselt number is an increasing monotonic function of $B$.

Tables 4 and 5 display the values of the functions which allow one to evaluate both the mean Nusselt number, on account of Eq. (29), and the local Nusselt number, by employing Eq. (27). The tables refer to $\sigma = 1.2$, $Pe = 100$, $\gamma = 0.5$ and $\gamma = 3$ and to different values of $B$. Table 4 shows that the real part of the interface complex temperature is a decreasing monotonic function of $B$, while the imaginary part of that complex-valued function is negative and is an increasing function of $B$.

Table 3
Analytical solution: values of the average Nusselt number versus the parameter $B$

| $B$ | $\overline{Nu}$ | $B$ | $\overline{Nu}$ |
|---|---|---|---|
| 1 | 2.06164 | 50 | 3.50071 |
| 2 | 2.07002 | 100 | 4.32306 |
| 5 | 2.12578 | 200 | 5.38193 |
| 10 | 2.29181 | 300 | 6.13304 |
| 20 | 2.68724 | 400 | 6.73414 |
| 30 | 3.01556 | 500 | 7.24336 |
| 40 | 3.27828 | 1000 | 9.09812 |

Table 4
Analytical solution: values of $\theta_1(1)$ and $\theta_2(1)$ as functions of $B$, for $Pe = 100$ and $\sigma = 1.2$

| $B$ | $\theta_1(1)$ | $\theta_2(1)$ | $\theta_1(1)$ | $\theta_2(1)$ |
|---|---|---|---|---|
| | $\gamma = 0.5$ | | $\gamma = 3$ | |
| 1 | 0.805956 | −0.223895 | 0.972680 | −0.0505939 |
| 2 | 0.669677 | −0.202655 | 0.938243 | −0.0609935 |
| 5 | 0.579269 | −0.142404 | 0.901938 | −0.0544579 |
| 10 | 0.534822 | −0.135044 | 0.883931 | −0.0580454 |
| 20 | 0.473818 | −0.139090 | 0.857889 | −0.0704374 |
| 50 | 0.389266 | −0.131232 | 0.809250 | −0.0858362 |
| 100 | 0.328844 | −0.120726 | 0.759060 | −0.0959843 |
| 200 | 0.268757 | −0.105292 | 0.680571 | −0.0996490 |
| 500 | 0.176083 | −0.0706261 | 0.464651 | −0.0723174 |
| 1000 | 0.0854228 | −0.0316550 | 0.202676 | −0.0265620 |

The analytical solution and the numerical solution described in the preceding sections display a very good agreement, as it is shown in Table 6. This table displays a comparison between val-

Table 5
Analytical solution: values of $\varphi_1$ and $\varphi_2$ as functions of $B$, for $Pe = 100$ and $\sigma = 1.2$

| $B$ | $\varphi_1$ | $\varphi_2$ | $\varphi_1$ | $\varphi_2$ |
|---|---|---|---|---|
| | $\gamma = 0.5$ | | $\gamma = 3$ | |
| 1 | −0.485105 | −0.559738 | −0.409769 | −0.758909 |
| 2 | −0.825791 | −0.506641 | −0.926243 | −0.914907 |
| 5 | −1.05174 | −0.356023 | −1.47023 | −0.816896 |
| 10 | −1.16260 | −0.337654 | −1.73826 | −0.870797 |
| 20 | −1.31416 | −0.347910 | −2.12080 | −1.05712 |
| 50 | −1.51943 | −0.329173 | −2.79584 | −1.29183 |
| 100 | −1.65037 | −0.305829 | −3.36316 | −1.45891 |
| 200 | −1.72721 | −0.277122 | −3.86004 | −1.57362 |
| 500 | −1.54929 | −0.231836 | −3.61222 | −1.42433 |
| 1000 | −0.935551 | −0.164181 | −1.96445 | −0.826596 |

Table 6
Comparison between analytical and numerical (*italic*) solution: values of the mean Nusselt number as function of $B$; values of the oscillation amplitude of the interface temperature and of the interface heat flux, for $Pe = 100$ and $\sigma = 1.2$

| $B$ | $\overline{Nu}$ | $\lvert\psi(1)\rvert$ $\gamma = 0.5$ | $\lvert\psi(1)\rvert$ $\gamma = 3$ | $\lvert\phi\rvert$ $\gamma = 0.5$ | $\lvert\phi\rvert$ $\gamma = 3$ |
|---|---|---|---|---|---|
| 1 | 2.06164 | 0.836477 | 0.973995 | 0.740698 | 0.862470 |
| | *2.063* | *0.8363* | *0.9740* | *0.7404* | *0.8631* |
| 2 | 2.07002 | 0.699669 | 0.940223 | 0.968822 | 1.30191 |
| | *2.071* | *0.6996* | *0.9402* | *0.9689* | *1.302* |
| 5 | 2.12578 | 0.596516 | 0.903580 | 1.11036 | 1.68194 |
| | *2.129* | *0.5965* | *0.9036* | *1.110* | *1.682* |
| 10 | 2.29181 | 0.551608 | 0.885835 | 1.21064 | 1.94418 |
| | *2.297* | *0.5515* | *0.8858* | *1.211* | *1.945* |
| 20 | 2.68724 | 0.493811 | 0.860776 | 1.35943 | 2.36966 |
| | *2.708* | *0.4935* | *0.8606* | *1.360* | *2.371* |
| 50 | 3.50071 | 0.410792 | 0.813790 | 1.55468 | 3.07986 |
| | *3.556* | *0.4097* | *0.8129* | *1.556* | *3.086* |
| 100 | 4.32306 | 0.350305 | 0.765105 | 1.67847 | 3.66596 |
| | *4.393* | *0.3477* | *0.7626* | *1.680* | *3.685* |

ues of the oscillation amplitude of the interface dimensionless temperature, of the interface dimensionless heat flux as well as of the mean Nusselt number. The values obtained analytically are written in roman, while those evaluated numerically are in italic. The discrepancies between the values obtained analytically and numerically are less that 0.8% for the oscillation amplitude of the interface temperature and of the interface heat flux, while rise up to 1.6% for the mean Nusselt number. In fact, numerical integration does not lead to an accurate evaluation of the mean Nusselt number due to the singular values in correspondence of the longitudinal positions $\zeta_n$ (Eq. (28)). Thus, the mean Nusselt number has been evaluated from Eq. (30) where, according to Eq. (11), one has $\theta_1(1) = \theta(1, \pi\, Pe/(2B))$, $\theta_2(1) = \theta(1, 0)$.

In Figs. 5 and 6, the longitudinal temperature distribution on the external wall ($\eta = \sigma$) is reported together with the dimensionless interface temperature at $\eta = 1$ and with the dimensionless interface heat flux. Fig. 5 refers to the case $\gamma = 0.5$, while Fig. 6 refers to $\gamma = 3$. In the case $\gamma = 0.5$, the interface temperature shows a $0.06\pi$ spatial shift forward and the heat flux shows a $0.11\pi$ spatial shift backward, both with respect to the external temperature. In the case of $\gamma = 3$, the interface temperature shows a $0.04\pi$ spatial shift forward and the heat flux shows a $0.13\pi$ spatial shift backward with respect to the external temperature. On the contrary, the spatial shift between the temperature and the heat flux at the interface does not change apparently with $\gamma$ and is equal to $0.17\pi$ in both situations. The dimensionless temperature distribution for the cases considered in Figs. 5 and 6 are plotted in Figs. 7 and 8 respectively. In these figures, the solid line identifies the solid–fluid interface. As it can be noticed, the continuity of the temperature at the interface is well ensured by the model. Furthermore, a lower conductivity wall ($\gamma = 0.5$) produces, in the solid region, a forward spatial shift of the temperature larger than that of a higher conductivity wall ($\gamma = 3$).

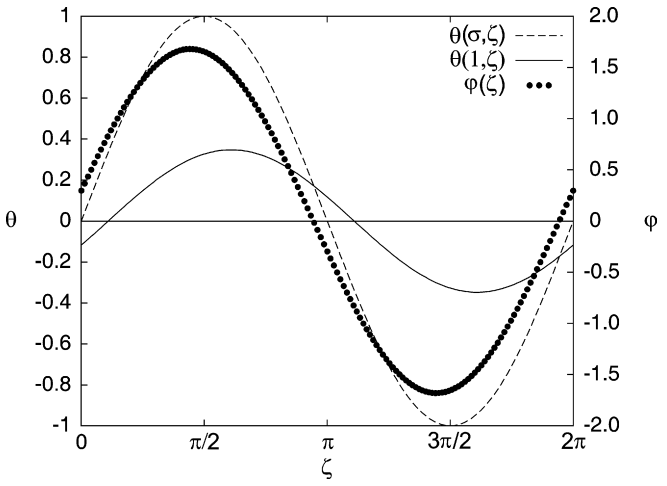


Fig. 5. Numerical solution: temperature distribution on the external wall $\eta = \sigma$; interface temperature at $\eta = 1$; dimensionless heat flux; for $\sigma = 1.2$, $\gamma = 0.5$, $Pe = 100$ and $B = 100$.

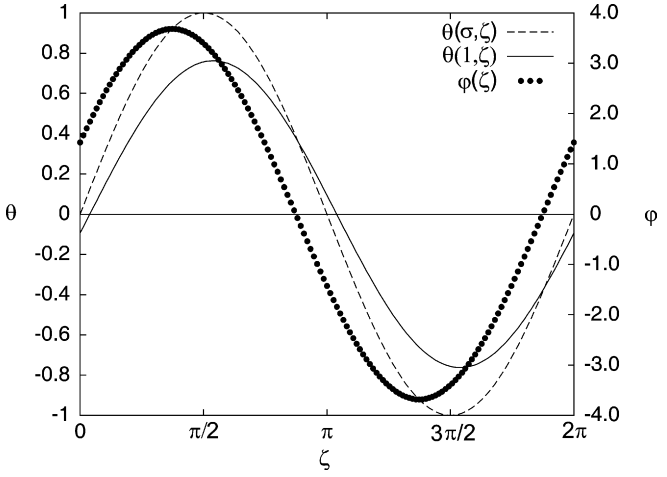


Fig. 6. Numerical solution: temperature distribution on the external wall $\eta = \sigma$; interface temperature at $\eta = 1$; dimensionless heat flux; for $\sigma = 1.2$, $\gamma = 3$, $Pe = 100$ and $B = 100$.

## 6. Conclusions

In the present paper, the conjugate heat transfer problem has been studied for the laminar forced convection of a fluid in a parallel-plane channel. The channel walls have finite width,

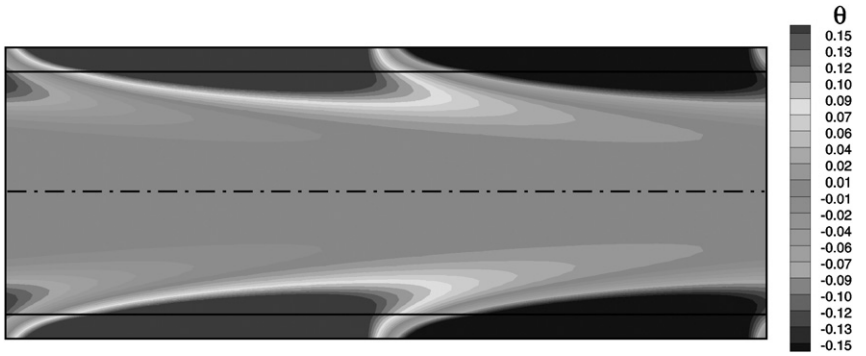


Fig. 7. Numerical solution: temperature distribution in the conjugate domain, for $\sigma = 1.2$, $\gamma = 0.5$, $Pe = 100$ and $B = 100$.

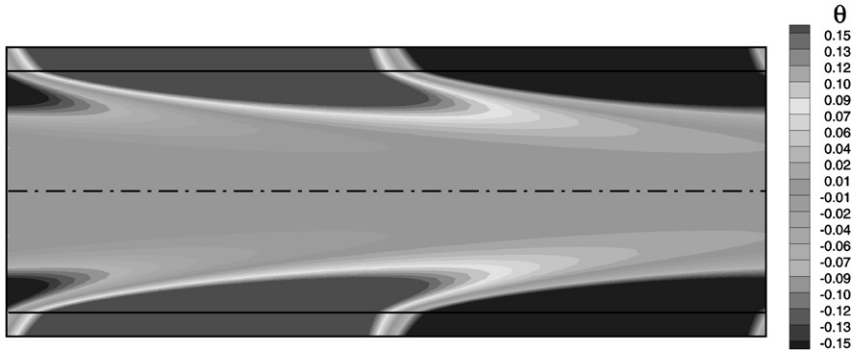


Fig. 8. Numerical solution: temperature distribution in the conjugate domain, for $\sigma = 1.2$, $\gamma = 3$, $Pe = 100$ and $B = 100$.

and the temperature on the external boundaries varies longitudinally with sinusoidal law. The local energy balance equation has been solved both analytically and numerically, with reference to the thermally developed region. Under this hypothesis, the temperature distribution is a periodic function of the longitudinal coordinate and the period is equal to the period of the prescribed wall temperature distribution. The analytical and numerical solutions have displayed a very good agreement and have evidenced the following features.

- The oscillation amplitude of the temperature field decreases for increasing values of the dimensionless angular frequency $B$.
- The mean Nusselt number in a longitudinal period is affected by singularities: indeed, for every longitudinal period there exists two axial positions where the bulk temperature and the interface solid–fluid temperature assume the same value.

## References

[1] C.-J. Hsu, Heat transfer in a round tube with sinusoidal wall heat flux distribution, AIChE J. 11 (1965) 690–695.
[2] S. Hasegawa, Y. Fujita, Turbulent heat transfer in a tube with prescribed heat flux, Int. J. Heat Mass Transfer 11 (1968) 943–962.
[3] A.J. Pearlstein, B.P. Dempsey, Low Peclet number heat transfer in a laminar tube flow subjected to axially varying wall heat flux, ASME J. Heat Transfer 110 (1988) 796–798.
[4] J.N.N. Quaresma, R.M. Cotta, Exact solutions for thermally developing tube flow with variable wall heat flux, Int. Comm. Heat Mass Transfer 21 (1994) 729–742.
[5] A. Barletta, E. Zanchini, Laminar forced convection with sinusoidal wall heat flux distribution: axially periodic regime, Heat Mass Transfer 31 (1995) 41–48.
[6] A. Barletta, E. Rossi di Schio, Periodic forced convection with axial heat conduction in a circular duct, Int. J. Heat Mass Transfer 43 (2000) 2949–2960.
[7] G. Comini, S. Del Giudice, C. Nonino, Finite Element Analysis in Heat Transfer, Taylor & Francis, Washington, DC, 1994.
[8] G. Comini, G. Cortella, M. Manzan, A streamfunction-vorticity-based finite-element formulation for laminar-convection problems, Numer. Heat Transfer B 28 (1995) 1–22.
[9] C. Nonino, G. Comini, An equal-order velocity–pressure algorithm for incompressible thermal flows. Part 1: formulation, Numer. Heat Transfer B 32 (1997) 1–15.
[10] C. Nonino, G. Comini, Finite element analysis of convection problems in spatially periodic domains, Numer. Heat Transfer B 34 (1998) 361–378.
[11] G. Comini, C. Nonino, S. Savino, Convective heat and mass transfer under dehumidifying conditions, in: R. Bennacer (Ed.), Progress in Computational Heat and Mass Transfer, Editions TEC and COC-Lavoisier, Paris, 2005, pp. 711–722.
[12] C.J. Roy, Review of code and solution verification procedures for computational simulation, J. Comput. Phys. 205 (2005) 131–156.